ARTICLE

Synthesis of hybrid tin halide perovskite solar cells with less hazardous solvents: methanol and 1,4-dioxane

Enrico Greul,[a] Pablo Docampo[b] and Thomas Bein*[a]

Dedicated to Wolfgang Schnick at the occasion of his 60th birthday.

Abstract: The toxicity of lead and the solvents utilized during the synthesis of hybrid halide perovskite films are potential obstacles for widespread applications of solar cell technology based on these materials. Alternatives such as those based on lead-free Sn-based devices often suffer from poor film morphologies, thus precluding competitive device efficiencies. Here, we demonstrate a new one-step route deploying mixtures of the less hazardous methanol and 1,4-dioxane for preparing high-quality methylammonium tin iodide films. We propose that the fast evaporation of these solvents is a key factor for film formation and show that the solvent ratio is essential to obtain phase pure, high-quality films. This leads to devices which outperform those prepared by conventional routes, likely due to a decreased defect density as confirmed with time-resolved photoluminescence measurements. Our results provide a further step towards non-hazardous synthesis routes for Sn-based optoelectronic devices.

Introduction

The constant increase of global energy consumption accompanied by the decline of fossil fuels generates a strong demand for new, sustainable energy sources.[1] In the past few years, organic-inorganic lead halide perovskites have emerged as highly efficient and inexpensive absorber materials for solar cells.[2,3] The simple processability and high power conversion efficiencies of over 20 % for state-of-the-art devices, assembled with methylammonium lead iodide ($MAPbI_3$), make these materials interesting candidates for large-scale applications.[4–6]
Due to the solubility of the lead salts in water, the toxicity of high-performing hybrid halide perovskites can be considered as a major barrier for commercializing this technology. Therefore, a great deal of effort has been undertaken to develop lead-free perovskite-related compounds based on Ge^{2+}, Sn^{2+}, Bi^{3+}, Sb^{3+} or Cu^{2+} for photovoltaic applications.[7–11] Sn-based compounds with the general formula $ASnX_3$, where A can be Cs, methylammonium (MA) or formamidinium (FA) and X can be I, Br, Cl or F, are the most promising alternatives to lead-based materials, with reported power conversion efficiencies (PCE) of ~ 6 % for devices based on methylammonium tin iodide ($MASnI_3$) films.[12,13] The lower efficiencies compared to lead-based materials are generally assigned to Sn^{4+} self-doping due to the facile oxidation of Sn^{2+} under ambient conditions.[13–17]
Further toxicity concerns arise from the harmful solvents utilized during the preparation of the perovskite films. The most common solvent, N,N-dimethylformamide (DMF), is known to be strongly hepatotoxic, even at relatively low concentrations, and the European Union has classified it as toxic to reproduction.[18–21] Furthermore, it can easily be taken up by dermal absorption, which is troubling since the dwell time of DMF in the body is much longer for percutaneous uptake than for pulmonary ingestion.[22] The second widespread solvent, dimethylsulfoxide (DMSO), although not acutely toxic, can induce bradycardia, respiratory problems, and alterations in blood pressure.[23,24] Furthermore, it potentially alters the chemical structure of cell membranes and thus their functional properties.[25] However, the most critical property of DMSO is that it can serve as an efficient carrier for other agents by enhancing the penetration through skin tissue, which is particularly critical for toxic substances like soluble lead compounds.[26]
With the prospect of possible commercialization of solution-processable solar cells, the development of less toxic film formation routes is an important issue to minimize the health risks during the film preparation. This must be balanced with the formation of homogenous films which uniformly cover the substrate. Considering Pb-based solar cells, the development of advanced film formation methods has led to homogeneous, smooth and pinhole-free perovskite films and has been the driving factor behind the great leaps in device efficiency.[27] Accordingly, the synthesis of high-quality $MASnI_3$ films can be considered as a key task to enable the system for high-efficiency photovoltaic applications.
$MASnI_3$ forms very rough and inhomogeneous films with micron-sized pinholes when employing common deposition methods based on DMF due to the much faster crystallization process as compared to $MAPbI_3$,. This, in turn, results in severely shunted photovoltaic devices. [12,13,15,28,29] In order to resolve these issues, Hao *et al*. developed a deposition route based on a (DMSO)-SnI_2 intermediate phase which improved the surface coverage by slow crystallization of the perovskite.[30] An alternative route was developed by Yokoyama *et al*. who adapted the well-known vapour-assisted solution process for the preparation of homogeneous but not crack-free $MASnI_3$ films.[31,32] Recently, Long *et al.* have developed a synthetic route for high-quality $FASnI_3$ films based on antisolvent dripping.[33] However, all three methods still rely

* Prof. Dr. T. Bein
Tel.: + 49-89-2180-77623 or -77621
E-Mail: thomas.bein@cup.uni-muenchen.de
[a] Department of Chemistry and Center for NanoScience (CeNS)
University of Munich (LMU)
Butenandtstr. 5−13 (E), 81377 Munich, Germany
[b] School of Electrical and Electronic Engineering
Newcastle University
Merz Court upon Tyne NE1 7RU Newcastle, UK

Supporting information for this article is given via a link at the end of the document.

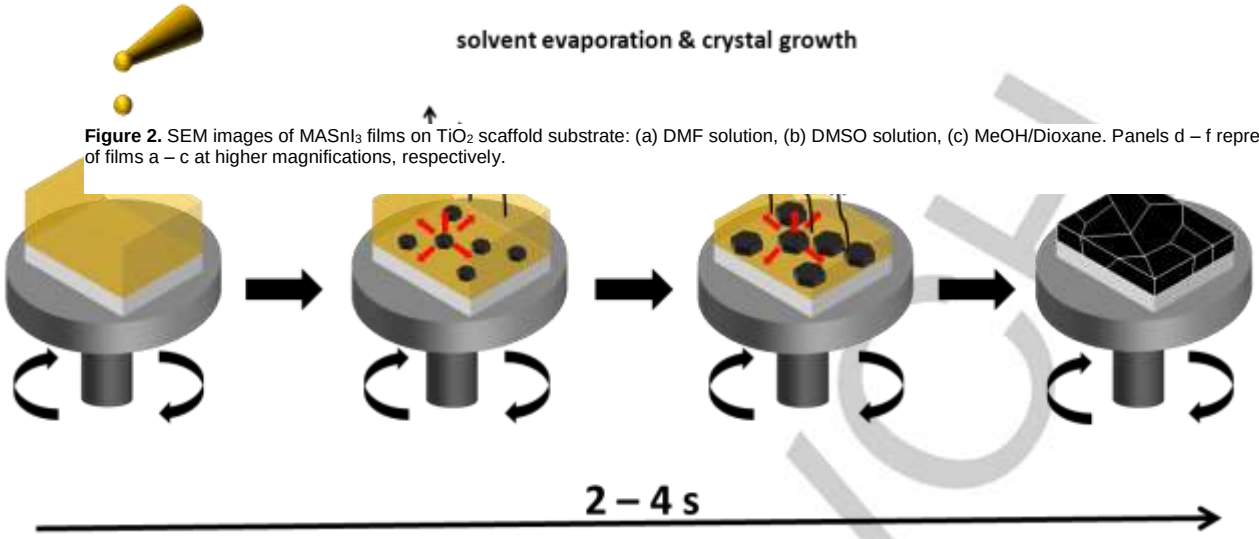

Figure 1. Schematic of the MeOH/Dioxane route. For simplification, only a few crystallites are depicted. The arrow underneath indicates the time range within which film formation usually occurs.

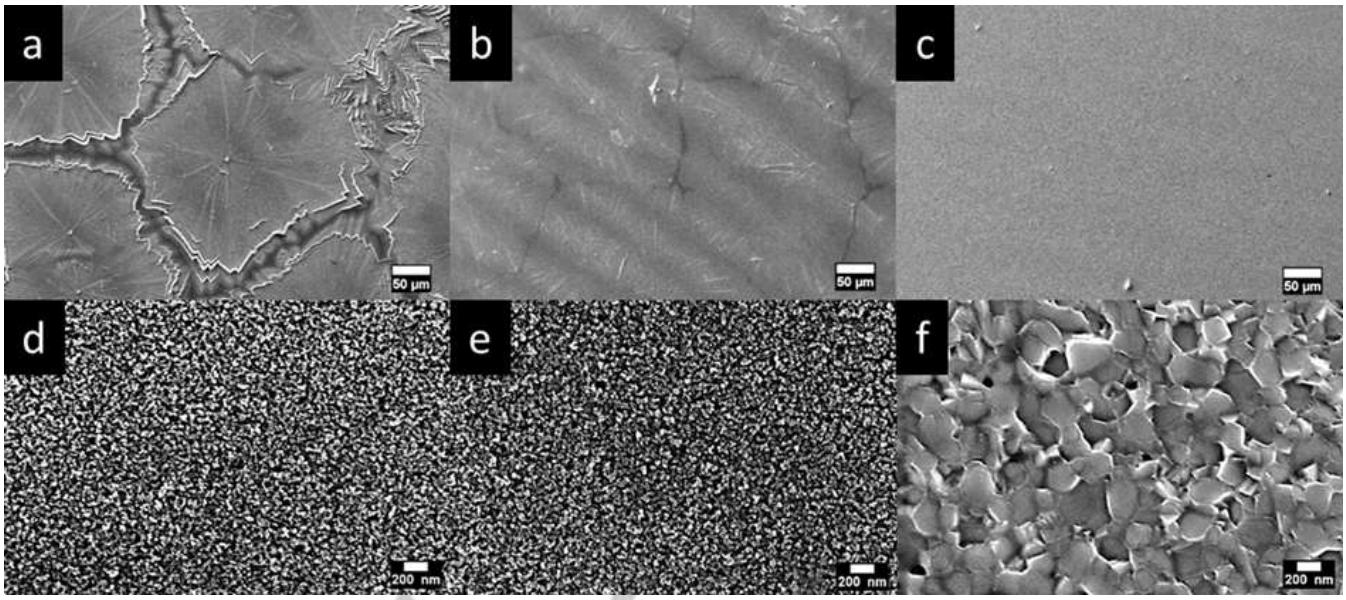

Figure 2. SEM images of $MASnI_3$ films on TiO_2 scaffold substrate: (a) DMF solution, (b) DMSO solution, (c) MeOH/Dioxane. Panels d – f represent SEM images of films a – c at higher magnifications, respectively.

on the hazardous DMF or DMSO solvents to deposit the metal halide layer. Previous studies on lead based hybrid perovskites showed that the hazardous solvents can be replaced by water to deposit the metal halide layer.[34,35] However, due to the sensitivity of the Sn^{2+} ion to oxygen and moisture this approach cannot be transferred to the lead-free compound.[13]

Here, we demonstrate a new one-step synthesis route for the preparation of high-quality, lead-free $MASnI_3$ films for photovoltaic applications based on less hazardous solvents (methanol (MeOH) and 1,4-dioxane (Dioxane)). Our route provides high quality films which outperform conventional one-step synthesis routes based on DMF and DMSO in photovoltaic devices. Our results represent a further step towards efficient lead-free perovskite based solar cells manufactured under non-dangerous conditions.

Results and Discussion

Our films were prepared on a 250 nm thick titanium dioxide (TiO_2) scaffold via a one-step spin-coating process from precursors dissolved in a MeOH: Dioxane mixture. As a reference, we also prepared $MASnI_3$ films utilizing the most common conventional one-step routes according to literature.[12,30]

When employing our newly developed MeOH/Dioxane route, the perovskite film forms within a few seconds after application of the solution, as depicted schematically in Figure 1. Since MeOH and Dioxane feature rather high vapour pressures of 130 hPa[36] and 37 hPa[37] at 20 °C, rapid solvent evaporation is expected. Accordingly, we propose that the fast supersaturation of the perovskite solution leads to the formation of a large number of small nuclei, resulting in smooth and homogeneous $MASnI_3$ films after complete solvent evaporation. Due to the faster crystallization of $MASnI_3$ compared to $MAPbI_3$, the rapid solvent

evaporation is essential to inhibit the growth of large, pointy crystals which protrude from the substrate and lead to substantial pinholes in the hole transporting layer (HTL).

Scanning electron microscopy (SEM) images revealed large differences in the morphology of $MASnI_3$ films made from the different solvents. As shown in Figure 2a, films prepared from a DMF solution are inhomogeneous, featuring a pattern of large $MASnI_3$ grains with low surface coverage. Figure 2b shows the SEM image of a $MASnI_3$ film made from a DMSO solution featuring enhanced homogeneity with less prominent patterns compared to films prepared from DMF solution. However, films made by our newly developed MeOH/Dioxane method (Figure 2c) exhibit films that fully cover the substrate with no visible pinholes or large protruding crystals, similar to those prepared by Long *et al*. via their developed antisolvent dripping route.[33]

Higher magnifications of the depicted films (Figure 2d-f) reveal striking morphology differences. In the films manufactured from the conventional solvents DMF and DMSO (Figure 2d,e) the porous TiO_2 scaffold is directly visible. In contrast, the film prepared from MeOH/Dioxane features a dense, homogeneous $MASnI_3$ capping layer exhibiting many relatively small crystallites, which supports our proposed film formation mechanism. In contrast with 2-step deposition methods that result in small cuboid crystals, the MeOH:Dioxane route yields a smooth capping layer consisting of non-regular-shaped crystals, similar to those from Yokoyama *et al.*[32] This dense capping layer is an important feature of high-efficiency perovskite solar cells,[38] as it prevents the direct contact of the HTL with the electron-transporting TiO_2.

The key enabler of the developed route based on less hazardous solvents is possible due to the higher solubility of SnI_2 in alcohols compared to PbI_2.[29] However, simply employing MeOH, which showed the highest solubility for $MASnI_3$ during our studies, leads to rather low concentrations of ~ 0.1 M. The addition of a miscible co-solvent that can complex with Sn(II) in the form of Dioxane, greatly increases the saturation concentration of the precursor mixture up to ~0.3 M.[39,40]

To gain more knowledge about the influence of Dioxane during the film formation, we prepared perovskite solutions with 25 % (v/v), 50 % (v/v) or 75 % (v/v) of Dioxane at a given $MASnI_3$ concentration of 0.3 M. We observed a decreasing solubility of the perovskite with higher concentrations of Dioxane, eventually leading to the formation of a black $MASnI_3$ precipitate at the highest concentration (see Figure 3a), confirmed by PXRD measurements (see Figure 3b).

Since highly polar solvents are commonly used to dissolve $MASnI_3$, it is likely that the reduction of the solubility is due to the small dipole moment of Dioxane.[41] This, in turn, suggests that the enhanced solubility of $MASnI_3$ in the MeOH/Dioxane solvent mixture at low Dioxane concentrations is not caused by the good solubility of the perovskite in Dioxane, but rather by the coordination of the solvent to Sn(II).[38,39] Since stable Sn(II)-(Dioxane) complexes are known for $SnCl_2$[40] and $SnBr_2$[39], we propose an inhibited reaction of MAI with SnI_2 to $MASnI_3$ in solution by the formation of Sn(II)-(Dioxane) adducts, resulting in an increased solubility of $MASnI_3$ in the utilized solvent mixture. The perovskite films form within a few seconds because of the high vapour pressure of the utilized solvents, and therefore a direct proof for the proposed Sn(II)-(Dioxane) adduct by commonly used FTIR measurements is not possible.

In order to address this, we performed PXRD measurements to obtain an indirect indication of the adduct, as shown in Figure 3b. Here, we observe additional reflections at the highest Dioxane concentration, which can be assigned to SnI_2. This is likely caused by the stabilization of the Sn(II)-(Dioxane) adduct at high Dioxane concentrations, which prevents its complete reaction with MAI to $MASnI_3$. Accordingly, we found an optimum in film quality and no phase segregation for 25 % (v/v) Dioxane. Thus, only the $MASnI_3$ film properties made from solutions containing 25 % (v/v) Dioxane are discussed in the following.

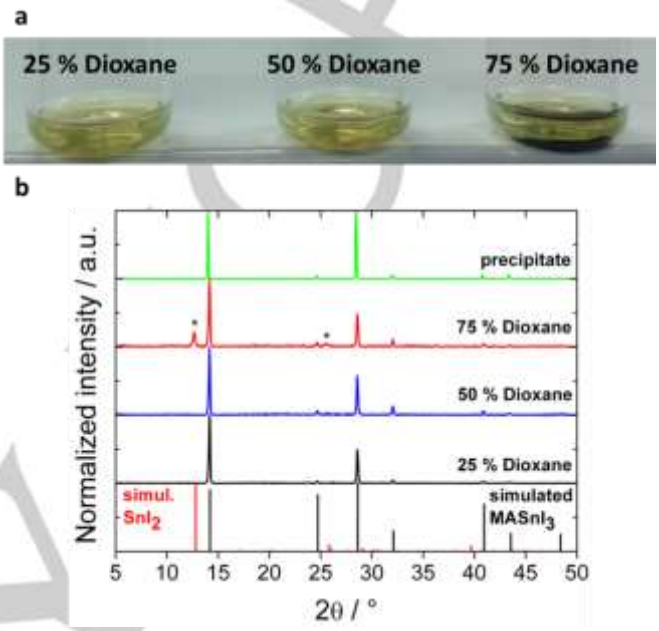

Figure 3. (a) Images of solutions prepared with 25 % (v/v), 50 % (v/v) or 75 % (v/v) Dioxane. The black precipitate can clearly be seen for the highest Dioxane concentration. (b) PXRD pattern of $MASnI_3$ films prepared from precursor solutions containing the three different Dioxane concentrations. The simulated patterns for $MASnI_3$ (black) and SnI_2 (red) are also given. Additionally, the PXRD pattern of the precipitate obtained from the solution with the highest Dioxane concentration is depicted (green).

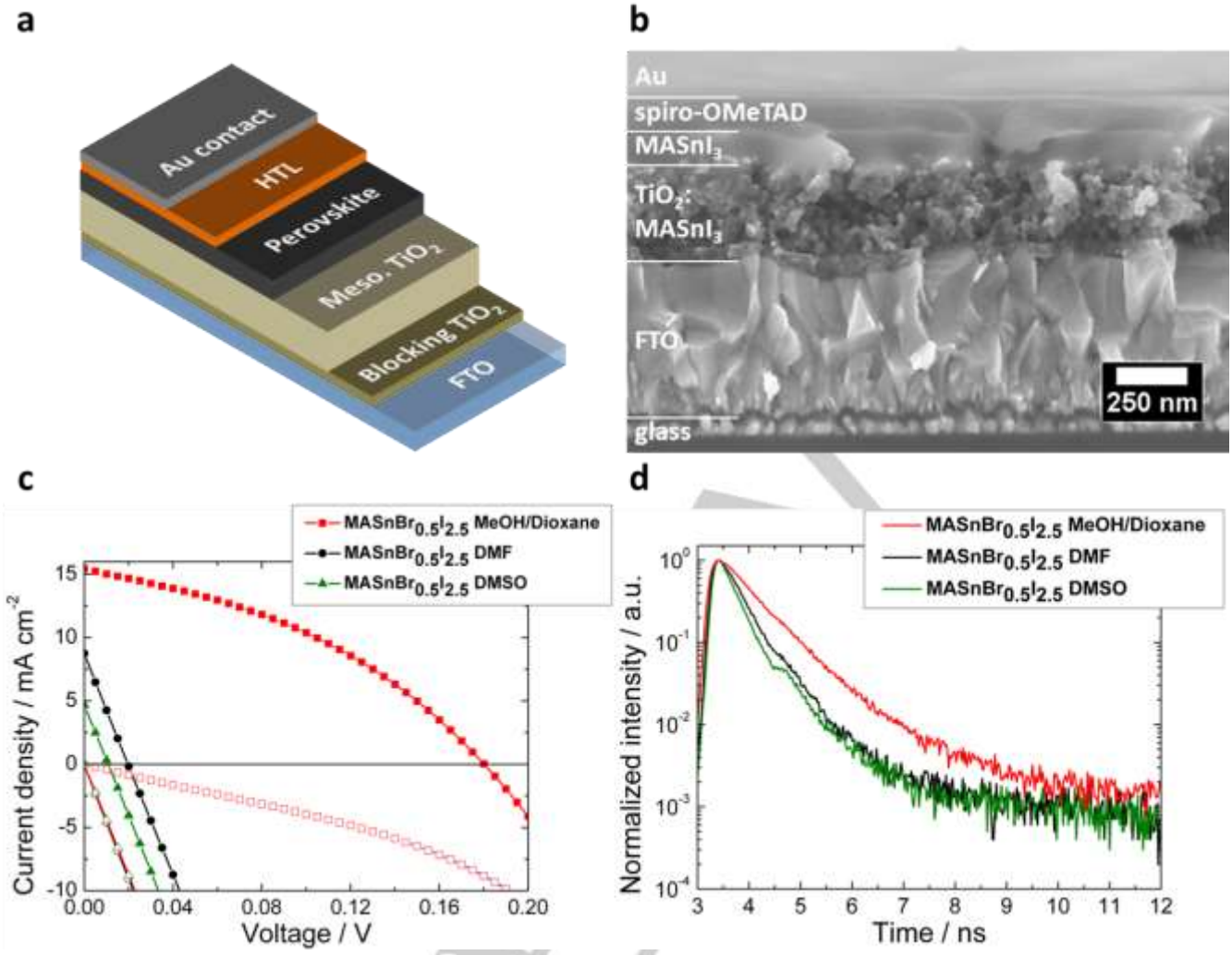

Figure 4. (a) Schematic of an assembled solar cell. (b) Cross-sectional SEM image of a functional device assembled with a MeOH/Dioxane $MASnI_3$ film. (c) Current-voltage characteristic showing the dependence of device performance on the deposition route. Hollow symbols refer to dark current traces (d) Time-resolved photoluminescence measurements of $MASnBr_{0.5}I_{2.5}$ films made from DMF, DMSO and MeOH/Dioxane solution.

We investigated the influence of the three different film formation methods (Sn-perovskite films prepared either from DMF, DMSO or MeOH/Dioxane solutions) on the photovoltaic properties by incorporating the resulting films in devices with the typical layer assembly of fluorine doped tin oxide (FTO)/compact-TiO_2/mesoporous-TiO_2/perovskite/HTL/Au contact.[31] A schematic of the solar cells and a cross-sectional image of a functional MeOH/Dioxane-derived device utilizing 2,2',7,7'-tetrakis-(N,N-di-pmethoxyphenylamine)9,9'-spirobifluoren (spiro-OMeTAD) as HTL are given in Figure 4a and 4b. The $MASnI_3$ capping layer on top the mesoporous-TiO_2 can clearly be seen, which is a a feature of high efficiency devices as it prevents shunting paths in devices. [13,32]

In order to further improve the device performance, we partially substituted iodide by bromide, which leads to a slightly smaller unit cell due to the smaller bromide without changing the tetragonal structure of the perovskite (see Figure S4). Hao *et al*. showed that bromide has a beneficial effect on the device performance, mainly due to the reduction of the series resistance R_S and the increase of the V_{OC}.[12] Additionally, they showed that bromide enhances the lifetime of the photoexcited species by destabilizing Sn^{2+}/Sn^{4+} defects leading to an enhanced charge collection efficiency resulting in a higher J_{SC}.[42] In our case, we obtained the best performing devices from a perovskite composition of $MASnBr_{0.5}I_{2.5}$.

The current-voltage (*J-V*) curves of the best performing devices out of 36 individual solar cells per synthesis route are displayed in Figure 4c. We obtained consistently very poor performance for devices assembled with $MASnBr_{0.5}I_{2.5}$ films prepared from DMF or DMSO solutions. In this case, the *J-V* curves show severely shunted behavior and PCEs of 0.04 % and 0.01 %,with short-circuit currents (J_{SC}) of 8.84 mA/cm² and 4.67 mA/cm² and open-circuit voltages (V_{OC}) of 0.02 V and 0.01 V for the best devices, which is in good agreement with reported values by Hao *et al*. and Takamichi *et al*..[30, 32] In contrast, the solar cells obtained via the MeOH/Dioxane route exhibit an enhanced performance with the highest PCE of 1.05 % with a J_{SC} of 15.44 mA/cm², V_{OC} of 0.18 V and a FF of 38 %. We note that devices based on films prepared on the MeOH/Dioxane route show prominent hysteresis similar to that observed for photovoltaics based on lead halide perovskite, see Figure S6.[43–46]

While low, the performance of the MeOH/Dioxane based devices is still in the range of reported results on tin halide perovskite-based solar cells by Yokoyama *et al.* and Long *et al.* showing a best PCE of 1.86 % and 0.11 %, respectively.[32,33] This is likely a result of the encapsulation protocol which requires a long 12h curing period in a nitrogen atmosphere which lowers the device performance.[12] We note that our champion device exhibits an almost ten times higher PCE compared to that prepared by Long *et al.* while both devices feature very similar morphologies, pointing to the high sensitivity of tin halide based perovskite to the synthesis conditions.[33]

The V_{OC} value for devices featuring tin-based perovskites is heavily impacted by first order recombination due to intrinsic defects, such as Sn vacancies, which depend on the Sn^{4+} doping level.[13,28] Hence, it is essential to keep the Sn^{4+} doping level as low as possible. Previous studies revealed that commercially available SnI_2 already contains a significant amount of Sn^{4+} similar to the precursor purchased for our studies.[12] Additionally, it has been shown that a voltage loss is also incurred due to the misalignment of the conduction band (CB) of the Sn-perovskite and the CB of TiO_2.[30,32]

In an effort to reduce the defect density, we purified the starting material according to the protocol established by Hao *et al*.[30,32] However, in our lab, we found no enhancement in the performance, see Figure S7. Another approach to reducing the defect density is the use of an excess of SnF_2 as reducing agent. Due to the very low solubility of SnF_2 in our solvent mixture, we could not observe an effect on device performance. However, since the highest reported PCE values for $MASnI_3$ based devices were obtained without the addition of SnF_2, we strongly believe that the new MeOH/Dioxane route holds promise for better-performing devices.

Further information about defects in the perovskite materials can be gained through time-resolved photoluminescence (PL) measurements.[13] Previous studies on Pb-based devices revealed that a long lifetime is associated with the presence of long-lived charge carriers, resulting in an increased charge extraction efficiency.[47,48] Similar studies on $MASnI_3$ yielded lifetimes of the photoexcited species of about 200 ps, being much shorter than for the lead-based counterpart[13,47,48] Here, we performed time-correlated single-photon counting (TCSPC) measurements on Sn-perovskite films prepared either from DMF, DMSO or MeOH/Dioxane solutions. All films show strong PL at around 840 nm (Figure S8), as expected. The corresponding PL decays are depicted in Figure 4d. All samples exhibit fast decays with the shortest lifetime values for perovskite films prepared from DMF solution (~310 ps) and DMSO solution (~260 ps), similar to previously reported values for $MASnI_3$.[13] The short lifetimes in these systems are typically assigned to the fast electron-hole pair recombination at Sn^{2+}/Sn^{4+} defect sites, most likely due to self-doping of the Sn-perovskite[13,16,41,49]. Surprisingly, the $MASnBr_{0.5}I_{2.5}$ film deposited from the MeOH/Dioxane route exhibits a significantly longer lifetime of the excited species of ~580 ps, indicating a lower defect density in the material. These TCSPC measurements provide a first indication that our newly developed MeOH/Dioxane route is suitable for preparing Sn-perovskite films with competitive photophysical properties.

Regarding toxicity concerns of the new MeOH/Dioxane route, both applied solvents represent less harmful alternatives to the commonly utilized solvents for perovskite film synthesis. Dioxane is a common solvent used in paints, varnishes, inks and dyes. Furthermore, it is a natural component in some food products, like tomatoes, shrimp and coffee. [50] Dioxane is, similar to DMSO, not classified as acutely toxic but animal experiments suggest a potentially carcinogenic effect, which could not be supported by studies on human workers exposed to occupational doses of Dioxane over decades.[50,51] Based on this, the International Agency for Research on Cancer (IARC) classified Dioxane as a 2B carcinogen just as carbon black and TiO_2, leading to the conclusion that Dioxane is not associated with cancer formation under common occupational conditions.[52,53]

MeOH is a widespread chemical for industrial applications, occurring naturally in humans, animals and plants. Excessive uptake of MeOH can cause blindness and death but the lethal dose is about twice as high as for DMF.[54,55] For occupational exposure not only the toxicity is important but also, the ability of the solvents to enter the body by different pathways. The effect of the different uptake pathways like oral ingestion, percutaneous absorption or inhalation on the body are important factors to assess the overall hazardousness. In particular, dermal absorption and inhalation of the solvents are of special interest, since these are considered to be the most likely uptake routes under occupational conditions.[56]

A comparison of the two solvents MeOH and Dioxane, utilized in our new synthesis route, with the commonly used solvents DMF and DMSO reveals that all solvents, except Dioxane, feature a high ability to penetrate through the skin, where DMSO exhibits, by far, the highest permeability rate among the mentioned solvents.[57–60] This high ability to penetrate through the skin tissue combined with their ability to act as an excellent carrier for a wide range of agents makes DMSO a much more critical solvent than Dioxane although both are not acutely toxic.[26] Furthermore, DMF and MeOH show very similar permeability rates, which means that both solvents have a similar ability to penetrate through the skin tissue.[57,58] Previous studies showed that dermal exposure to MeOH or DMF leads to increased concentrations of the particular chemical in the blood and urine of the experimental subjects.[57,58] Despite the very similar behaviour regarding dermal uptake, the degradation of the solvents in the body is very different. Chang *et al.* showed that dermal exposure to DMF of workers of a synthetic leather factory for several consecutive working days leads to a significant accumulation of the DMF body burden.[60] Although there is no comparable data available for MeOH, Battermann *et al.* revealed a clearance of MeOH in the body after dermal exposure of a few hours indicating the absence of MeOH accumulation in the body.[57] However, due to the high volatility of MeOH, the most probable uptake route is considered to be inhalation. Long-term studies on experimental subjects exposed to MeOH vapors for four consecutive days (8h/d) revealed no MeOH accumulation in the blood and urine of the experimental subjects at MeOH concentrations in the air slightly above the permissible exposure limit (PEL) of 260 mg/m^3 stated by the National Institute for Occupational Safety and Health (NIOSH).[54,61] Accordingly, the World Health Organization (WHO) considers MeOH as non-hazardous under occupational conditions, maintaining the PEL.[62]

In contrast, similar studies on DMF over a period of five consecutive days showed an accumulation of the toxic DMF metabolic product N-acetyl-S-(N-methylcarbamoyl)cysteine in the

blood and urine of the experimental subjects even at the PEL of 30 mg/m^3.[55,63] Furthermore, long-term exposure to DMF induces negative effects, like stomach pain, loss of appetite, nausea, headache and alcohol intolerance even at air concentrations below the PEL.[64,65] Accordingly, our new route based on MeOH and Dioxane can be regarded as a far less harmful synthesis route for the preparation of lead-free perovskite films.

Conclusions

In conclusion, we have demonstrated a new synthesis route for high-quality $MASnI_3$ films employing less hazardous solvents in an effort to address toxicity concerns. This new approach is based on the higher solubility of Sn(II) salts in alcoholic solvents compared to the usual lead compounds, which allowed us to deposit films from a MeOH/Dioxane mixture. Here, we found that the addition of Dioxane greatly enhances the solubility of SnI_2, essential to achieve films of several hundred nanometers in thickness, through the formation of Sn(II)-(Dioxane) adducts. Both MeOH and Dioxane feature high vapour pressures which, upon deposition and evaporation on the substrate, quickly lead to supersaturation of the precursor mixture and the formation of a large number of nuclei, leading to far smoother and homogeneous films than those prepared from conventional DMF or DMSO mixtures. Solar cells prepared with our new deposition route perform better than films prepared by conventional one-step routes, mainly due to the better film formation and fewer defects as indicated by time-resolved PL measurements. This opens a new avenue for more environmentally friendly and non-hazardous synthesis routes for perovskite-based solar cells.

Experimental Section

All chemicals were used as received without any further purification. All synthesis steps were conducted in a nitrogen-filled glove box to avoid oxidation of the Sn(II) compounds.

Substrate preparation: Fluorine-doped tin oxide (FTO)-coated glass sheets (7 Ωsq^{-1}, Pilkington, USA) were patterned by etching with zinc powder and 3 M HCl. They were subsequently cleaned with a 2% Hellmanex solution and rinsed with deionized water, ethanol, and acetone. Directly before applying the blocking layer, remaining organic residues were removed by an oxygen plasma treatment for 5 min. A compact titanium dioxide (TiO_2) layer was deposited by spin-coating a sol-gel precursor solution at 2000 rpm for 45 s followed by subsequent annealing at 500 °C for 45 min. For the sol-gel solution a 27.2 mM (70 µL) solution of HCl in 2-propanol (5 mL) was added dropwise to a vigorously stirred 0.43 mM (735 µL) solution of titanium isopropoxide (99.999%, Sigma–Aldrich) in 2-propanol (5 mL). Afterwards, a 250 nm thick, mesoporous TiO_2 layer was applied by spin-coating 100 µL of a TiO_2 nanoparticle paste (Dyesol DSL 18NR-T) diluted in absolute ethanol (1:3.5 weight ratio) onto the compact TiO_2 layer at 2500 rpm for 30 s followed by subsequent annealing at 500 °C for 15 min.

Perovskite film preparation

Method 1: MeOH/Dioxane. The precursor solution was prepared by dissolving 111.6 mg SnI_2 (99.999%, ultra dry, Alfa Aesar) in 1,4-dioxane (0.25 mL, Dioxane, anhydrous, 99.8 %, Sigma-Aldrich). In a second vial, either 48 mg of methylammonium iodide (MAI, Dyesol), for the pure iodide perovskite, or a mixture of 24 mg MAI and 17 mg methylammonium bromide (MABr, Dyesol), for the mixed halide perovskite, were dissolved in methanol (0.75 mL, MeOH, anhydrous, 99.8 %, Sigma-Aldrich). After complete dissolution of the organic precursor, the MeOH solution was added to the SnI_2 solution to dissolve the remaining SnI_2 completely. Subsequently, 100 µL of the precursor solution was spun onto the TiO_2-covered substrates at 3000 rpm for 15 s. The substrates were annealed at 70 °C for 10 min to remove possible solvent residues directly after spin-coating.

Method 2: DMF. The perovskite solution was prepared by dissolving 372 mg SnI_2 and 159 mg MAI for the pure iodide compound or a mixture of 80 mg MAI and 56 mg MABr, for the mixed halide perovskite, in N,N-dimethylformamide (1 mL, DMF, anhydrous, 99.8 %, Sigma-Aldrich). After mixing, the solution was placed on a hotplate at 100 °C in order to fully dissolve the tin precursor. 100 µL of the precursor solution were spun at 2000 rpm for 30 s onto a TiO_2-covered substrate with subsequent annealing at 100 °C for 10 min.

Method 3: DMSO. The procedure followed is the same as the previous procedure but using dimethylsulfoxide (DMSO, anhydrous, ≥99.9 %, Sigma-Aldrich) instead of DMF as the solvent. 100 µL of the precursor solution were spun at 4000 rpm for 30 s onto a TiO_2-covered substrate with subsequent annealing at 100 °C for 10 min.

Solar cell fabrication: After film formation, the films were covered with a hole transporting layer (HTL) of 2,2',7,7'-tetrakis-(N,N-di-pmethoxyphenylamine)9,9'-spirobifluorene (spiro-OMeTAD Borun Chemicals, 99.5% purity). The HTL solution was prepared by dissolving 73 mg of spiro-OMeTAD in chlorobenzene (1 mL, 99.8%, Sigma–Aldrich). The solution was filtered and mixed with 2,5-lutidine (30 µL, 98+%, Alfa Aesar), and a 520 mg mL^{-1} bis(trifluoromethane)sulfonamide lithium salt (LiTFSI, 99.95%, Sigma–Aldrich) solution in acetonitrile (17.5 µL). This solution was spin-coated dynamically at 1500 rpm for 45 s. In a second step the sample rotation was accelerated to 2000 rpm for 5 s to allow the solvent to dry completely. Finally, the 40 nm thick gold electrodes were evaporated thermally on top of the device. In order to prevent the perovskite film from oxidation, the devices were sealed by a 25 µm thick hot-melting polymer (Surlyn®) and a microscope coverslip. To provide a complete sealing, the edges of the microscope coverslip were treated with epoxy resin. The devices were stored for about 12 h before measuring under inert conditions to allow complete hardening of the epoxy resin.

Characterization methods: X-ray diffraction measurements on films and the powder sample of the precipitate were performed using a Bruker D8 Discover X-ray diffractometer operating at 40 kV and 30 mA, employing Ni-filtered Cu Kα radiation (λ = 1.5406 Å) and a position-sensitive detector (LynxEye) in reflection mode. All other powder x-ray pattern were obtained in transmission mode by a STOE Stadi MP diffractometer with a Cu Kα1 radiation source (λ = 1.54060 Å) operating at 40 kV and 40 mA. The diffractometer was equipped with a DECTRIS MYTHEN 1K solid-state strip detector. All samples were exposed to ambient conditions during the measurement. Scanning electron microscopy (SEM) cross-section images were acquired on a JEOL JSM-6500F microscope. The sample was fixed in a self-made sample holder. SEM top-view images were taken with a Carl Zeiss Ultra Plus scanning electron microscope. The sample was fixed by a sticky carbon pad. All SEM samples were exposed to ambient conditions not longer than one minute during the transfer procedure into the SEM. For the optical characterization, precursor solutions were prepared similarly as used for the devices. 100 µL of the solution was spun using the same conditions as utilized for solar cells onto a glass slide. Subsequently, the film was sealed by a glass coverslip and epoxy resin to avoid oxidation. Steady-state absorption spectra were acquired with a Lambda 1050 UV-Vis spectrophotometer (Perkin Elmer) using an integration sphere. Steady state and time-resolved PL measurements were performed with a Fluotime 300 Spectrofluorometer (Picoquant GmbH). The excitation wavelength was fixed at 510 nm. The emission for

time-resolved measurements was monitored at the maximum intensity of the steady state photo-emission. *J-V* curves were recorded with a Keithley 2400 source meter under simulated AM 1.5 sunlight, calibrated to 100 mW cm^{-2} with a Fraunhofer ISE certified silicon cell. The active area of the solar cells was defined with a square metal aperture mask of 0.0831 cm^2.

Acknowledgements

We thank Verena Hintermayr from the Physics Department of the University of Munich (LMU) for the top-view scanning electron microscopy measurements. We acknowledge funding by the Bavarian State Ministry of the Environment and Consumer Protection, the German Federal Ministry of Education and Research (BMBF) under the agreement number 01162525/1, the Bavarian network "Solar Technologies Go Hybrid", and the DFG Excellence Cluster Nanosystems Initiative Munich (NIM). We gratefully acknowledge support from the European Union through the award of a Marie Curie Intra-European Fellowship.

Keywords: tin • energy conversion • thin films • semiconductor • perovskite phases

[1] U.S. Energy Information Administration. Available online: http://www.eia.gov/todayinenergy/detail.cfm?id=12251 (accessed on 8 June 2017).
[2] A. Kojima, K. Teshima, Y. Shirai, T. Miyasaka, *J. Am. Chem. Soc.* **2009,** *131*, 6050.
[3] 3.J. M. Ball, M. M. Lee, A. Hey, H. J. Snaith, *Energy Environ. Sci.* **2013,** *6,* 1739.
[4] M. M. Lee, J. Teuscher, T. Miyasaka, T. N. Murakami, H. J. Snaith, *Science* **2012,** *338*, 643.
[5] J. Burschka, N. Pellet, S. J. Moon, R. Humphry-Baker, P. Gao, M. K. Nazeeruddin, M. Grätzel, M. *Nature* **2012,** *499*, 316.
[6] H. Zhou, Q. Chen, G. Li, S. Luo, T. B. Song, H. S. Duan, Z. Hong, Y. Jingbi Y. Yang, *Science* **2014,** *345*, 542.
[7] T. Krishnamoorthy, H. Ding, C. Yan, W. L. Leong, T. Baikie, L. Zhang, M. Sherburne, S. Li, M. Asta, N. Mathews, et al., *J. Mater. Chem. A* **2015,** *3*, 23829.
[8] B. W. Park, B. Philippe, X. Zhang, H. Rensmo, G. Boschloo, E. M. J. Johansson. *Adv. Mater.* **2015,** *27*, 6806.
[9] B. Saparov, F. Hong, J. P. Sun, H. S. Duan, W. Meng, S. Cameron, I. G. Hill, Y. Yan, D. B. Mitzi, *Chem. Mater*. **2015,** *27*, 5622.
[10] X. P. Cui, K. J. Jiang, J. H. Huang, Q. Q. Zhang, M. J. Su, L. M. Yang, Y. L. Song, X. Q. Zhou, *Synth. Met*. **2015,** *209*, 247.
[11] M. Lyu, J. H. Yun, M. Cai, Y. Jiao, P. V. Bernhardt, M. Zhang, Q. Wang, A. Du, H. Wang, G. Liu, L. Wang, *Nano Res.* **2016,** *9*, 692.
[12] F. Hao, C. C. Stoumpos, C. C. Cao, R. P. H. Chang, M. G. Kanatzidis, *Nat. Photonics* **2014,** *8*, 489.
[13] N. K. Noel, S. D. Stranks, A. Abate, C. Wehrenfennig, S. Guarnera, A. A. Haghighirad, A. Sadhanala, G. E. Eperon, S. K. Pathak, M. B. Johnston, A. Petrozza, L. M. Herz, H. J. Snaith, H.J. *Energy Environ. Sci.* **2014,** *7*, 3061.
[14] Y. Ogomi, A. Morita, S. Tsukamoto, T. Saitho, N. Fujikawa, Q. Shen, T. Toyoda, K. Yoshino, S. S. Pandey, T. Ma, et al., *J. Phys. Chem. Lett.* **2014,** *5*, 1004.
[15] M. H. Kumar, S. Dharani, W. L. Leong, P. P. Boix, R. R. Prabhakar, T. Baikie, C. Shi, H. Ding, R. Ramesh, M. Asta, et al., *Adv. Mater.* **2014,** *26*, 7122.
[16] Y. Takahashi, R. Obara, Z.Z. Lin, Y. Takahashi, T. Naito, T. Inabe, S. Ishibashi, K. Terakura, *Dalton Trans*. **2011,** *40*, 5563.
[17] F. Zuo, S. T. Williams, P. W. Liang, C. C. Chueh, C. Y. Liao, A. K. Y. Jen, *Adv. Mater.* **2014,** *26*, 6454.
[18] G. L. Jr. Kennedy, *Crit. Rev. Toxicol*. **1986,** *17*, 129.
[19] V. Scailteur, E. DeHoffmann, J. P. Buchet, R. Lauwerys, *Toxicol*. **1984,** *29*, 221.
[20] L. E. Fleming, S. L. Shalat, C. A. Redlich, *Scand J. Work Environ. Health* **1990,** *16*, 289.
[21] REACH-clp-biozid-helpdesk. Available online: http://www.reach-clp-biozidhelpdesk.de/de/ REACH/ Kandidatenliste/Listen/N,NDimethylformamid/ N,N-Dimethylformamid_content.html in german (accessed on 8 June 2017).
[22] J. Mráz, H. Nahová, *Int Arch Occup Environ. Health* **1992,** *64*, 79.
[23] D. Martin, H. Hauthal, *Dimethyl Sulphoxide*, New York: Worth, **1989**.
[24] M. B. Sulzberger, T. A. Cortese, L. Fishman, H. S. Wiley, P. S. Peyakovich, *Ann. New York Acad. Sci.* **1967,** *141*, 437.
[25] S. V. Rudenko, S. D. Gapochenko, U. A. Bondarenko, *Biophysics* **1984,** *29*, 245.
[26] G. Embery, P. H. Dugard, *J. Invest. Dermatol.* **1971,** *57*, 308.
[27] T. B. Song, Q. Chen, Zhou, C. Jiang, H. H. Wang, Y. M. Yang, Y. Liu, J. You, Y. Yang, *J. Mater. Chem. A* **2015,** *3*, 9032.
[28] M. H. Kumar, S. Dharani, W. L. Leong, P. P Boix, R. R. Prabhakar, T. Baikie, C. Shi, H. Ding, R. Ramesh, M. Asta, M. Graetzel, S. G. Mhaisalkar, N. Mathews, *Adv. Mater.* **2014,** *26*, 7122.
[29] K. Liang, D. B. Mitzi, M. T. Prikas, *Chem. Mater.* **1998,** *10*, 403.
[30] F. Hao, C. C. Stoumpos, P. J. Guo, N. J. Zhou, T. J. Marks, R. P. H. Chang, M. G. Kanatzidis, *J. Am. Chem. Soc.* **2015,** *137*, 11445.
[31] Q. Chen, H. P. Zhou, Z. R. Hong, S. Luo, H. S. Duan, H. H. Wang, Y.S. Liu, G. Li, Y. Yang, *J. Am. Chem. Soc.* **2013,** *136*, 622.
[32] T. Yokoyama, D. H. Cao, C. C. Stoumpos, T. B. Song, Y. Sato, S. Aramaki, M. G. Kanatzidis, *J. Phys. Chem. Lett.* **2016,** *7*, 776.
[33] L. Ji, T. Zhang, Y. Wang, P. Zhang, D. Liu, Z. Chen, S. Li, *Nanoscale Res. Let.* **2017,** *12*(1), 367.
[34] T.-Y. Hsieh, T.-C. Wei, K.-L. Wu, M. Ikegami, T. Miyasaka, *Chem. Commun.* **2015,** *15*, 13294.
[35] Y. Feng, K.-J. Jiang, J.-H. Huang, H.-J. Wang, M.-G. Chen, Y. Zhang, L. Zheng, Y.-L. Song, *Thin Solid Films* **2017,** *636*, 639.
[36] H. F. Gibbard, L. C. Jefferson, *J. Chem. Eng. Data* **1974,** *19*, 308.
[37] E. W. Reid, E. E. Hofmann, *J. Ind. Eng. Chem.* **1929,** *21*, 695.
[38] D. Bi, D. M. El-Zohry, A. Hagfeldt, G. Boschloo, *ACS Appl. Mater. Interfaces* **2014,** *6*, 18751.
[39] R. H. Andrews, J. D. Donaldson, E. Hough, D. G. Nicholson, *Acta. Cryst.* **1977,** *B33*, 307.
[40] E. Hough, D. G. Nicholson, *J. Chem. Soc. Dalton Trans.* **1976,** 1782.
[41] R. D. Jr. Nelson, D. R. Jr. Lide, A. A. Maryott, *Selected Values of Electric Dipole Moments for Molecules in the Gas Phase*, NSRDS-NBS 10, National Bureau of Standards, Washington, D. C. **1967**.
[42] M. G. Kanatzidis, F. Hao, *U.S. Patent Application* Nr. 14/686,539, **2015**.
[43] H. J. Snaith, A. Abate, J. M. Ball, G. E. Eperon, T. Leijtens, N. K. Noel, S. D. Stranks, J. T. W. Wang, K. Wojciechowski, W. Zhang, *J. Phys. Chem. Lett.* **2014,** *5*, 1511.
[44] E. L. Unger, E. T. Hoke, C. D. Bailie, W. H. Nguyen, A. R. Bowring, T. Heumüller, M. G. Christoforo, M. D. McGehee, *Energy Environ. Sci.*, **2014,** *7*, 3690.
[45] H. S. Kim, N. G. Park, *J. Phys. Chem. Lett*. **2014,** *5*, 2927.
[46] R. S. Sanchez, V. Gonzalez-Pedro, J. W. Lee, N. G. Park, Y. S. Kang, I. Mora-Sero, J. Bisquert, *J. Phys. Chem. Lett.* **2014,** *5*, 2357–2363.
[47] C. R. Kagan, D. B. Mitzi, C. D. Dimitrakopoulos, Science **1999,** *286*, 945.
[48] G. Xing, N. Mathews, S. Sun, S. S. Lim, Y. M. Lam, M. Grätzel, S. Mhaisalkar, T. C. Sum, *Science* **2013,** *342*, 344.
[49] Y. Takahashi, H. Hasegawa, Y. Takahashi, T. Inabe, *J. Solid State Chem.* **2013,** *205*, 39–.

[50] A. Stickney, S. L. Sager, J. R. Clarkson, L. A. Smith, B. J. Locey, M. J. Bock, R. Hartung, S. F. Olp, *Regul. Toxicol. Pharm.* **2003,** *38*, 183.
[51] R. J. Kociba, S. B. McCollister, C. Park, T. R. Torkelson, P .J. Gehring, *Toxicology App. Pharmacol.* **1974,** *30*, 275.
[52] Netherlands Organization for Applied Scientific Research (TNO) and the National Institute of Public Health and the Environment (RIVM). Chemical Substances Bureau, Ministry of Housing, Spatial Planning and the Environment (VROM) *Risk Assessment: 1, 4-Dioxane*. Final Version, 5 November, EINECS-No.: 204-661-8, Netherlands, **1999**.
[53] International Agency for Research on Cancer (IARC). Available online: http://monographs.iarc.fr/ENG/Classification/latest_classif.php (accessed on 9 June 2017).
[54] Centers for Desease Control and Prevention (CDC). Available online: http://www.cdc.gov/niosh/idlh/67561.html (accessed on 8 June 2017).
[55] Centers for Desease Control and Prevention (CDC). Available online http://www.cdc.gov/niosh/idlh/68122.html (accessed on 8 June 2017).
[56] C. E. Becker, *J. Emerg. Med*. **1983,** *1*, 51.
[57] S. A. Battermann, A. Franzblau, Int. Arch. *Occup. Environ. Health* **1997,** *70*, 341.
[58] H.-Y. Chang, C.-Y. Tsai, Y.-Q. Lin, T.-S. Shi, W.-C. Lin, *Occup. Environ. Med.* **2005,** *62*, 151.
[59] K. Dennerlein, D. Schneider, T. Göen, K. H. Schaller, H. Drexler, G. Korinth, *Toxicol. In Vitro* **2013,** *27*, 708.
[60] C. Ursin, C. M. Hansen, J. W. Van Dyk, P. O. Jensen, I. J. Christensen, J. Ebbehoej, *Am. Ind. Hyg. Assoc. J.* **1995,** *56*, 651.
[61] V. Šedivec, M. Mráz, J. Flek, *Int. Arch. Occup. Environ. Health* **1981,** *48*, 257.
[62] World Health Organization (WHO), International Programme On Chemical Safety (IPCS), *Methanol Health And Safety Guide*, No. 105, **1997**.
[63] J. Mraz, H. Nohova, *Int. Arch. Occup. Environ. Health* **1992,** *64*, 85.
[64] R. R. Lauwerys, A. Kivits, M. Lhoir, P. Rigolet, D. Houbeau, J. P. Buchet, H. A. Roels, *Int .Arch. Occup. Environ. Health* **1980,** *45*, 189.
[65] V. Scailteur, R. R. Lauwerys, *Toxicol.* **1987,** *43*, 231.

Entry for the Table of Contents (Please choose one layout)

Layout 1:

FULL PAPER

Text for Table of Contents

((Insert TOC Graphic here: max. width: 5.5 cm; max. height: 5.0 cm))

*Author(s), Corresponding Author(s)**

Page No. – Page No.

Title

Layout 2:

FULL PAPER

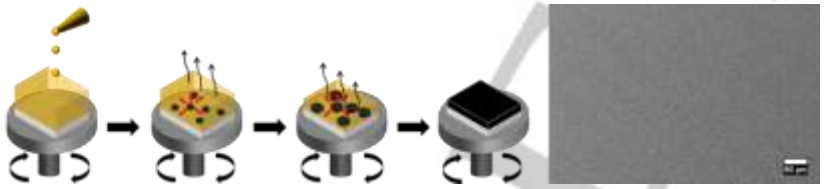

*E. Greul, P. Docampo, T. Bein **

Page No. – Page No.

Synthesis of hybrid tin halide perovskite solar cells with less hazardous solvents: methanol and 1,4-dioxane